STUDY OF INTEGRATION, DISTRIBUTION AND DEGRADATION OF SUGARCANE BAGASSE FIBER AS PARTIAL REPLACEMENT FOR FINE AGGREGATE IN CONCRETE SAMPLES

EDGAR ONOFRE BUSTAMANTE, ANA CECILIA ESPINDOLA-FLORES and ANA KAREN CÁRDENAS DE LA FUENTE

Instituto Politécnico Nacional-Centro de Investigación en Ciencia Aplicada y Tecnología Avanzada, Unidad Altamira, Km. 14.5 Carretera Tampico-Puerto Industrial Altamira, Altamira Tamaulipas CP 89290, Mexico

✉ *Corresponding author: E. Onofre Bustamante, eonofre@ipn.mx*

Received July 21, 2023

In this study, structural and morphological characterizations were carried out to evaluate the integration, distribution and degradation of sugarcane bagasse fiber (CBF) in a concrete matrix. The samples for evaluation were modified by adding CBF in 0.5% and 1% wt proportions. The modified concrete specimens were exposed to different aggressive conditions over four years before use. The chemical and structural properties of the modified samples were evaluated using Fourier transform infrared spectroscopy, X-ray diffraction and X-ray photoelectron spectroscopy, while the morphology, distribution and fiber degradation in the samples were determined using scanning electron microscopy and confocal laser scanning microscopy, respectively. The results obtained from spectroscopy and X-ray diffraction indicated the presence of cellulose, and showed a change in molecular orientation, which was attributed to the hydrolysis reaction. The microscopy analyses revealed that the CBF did not undergo degradation.

Keywords: sugarcane bagasse fiber, concrete, distribution, degradation, alkali-hydrolysis reaction

INTRODUCTION

Concrete is the most widely employed material in the construction industry, due to its excellent engineering properties.[1] If properly produced, concrete has exceptional durability and mechanical characteristics.[2] Currently, close to 4 billion tons of cement are produced worldwide annually, which has an impact in terms of natural resources.[3] Consequently, researchers are looking for alternatives or strategies to reduce this impact on natural resource depletion and the environment. In addition, there is a need to find a balance between industrial growth and the structural limits of the planet, and to ensure the competitiveness of this construction material. In view of this, new types of concrete that incorporate various type of fibers have been developed;[4] these are known as fiber-reinforced concrete (FRC), and can be defined as amalgamated materials made up of Portland cement and aggregates.

Several studies have demonstrated that biomass ash materials, such as rice husk ash, palm oil fuel, elephant grass and sugarcane bagasse,[5-14] among others, can be used as supplementary cementitious materials to replace part of the cement in ordinary concrete. It has been reported that the use of natural carbon-based fibers, a group of materials that can be used to structurally reinforce concrete, gives favorable results in terms of increasing the mechanical properties.[15-17] According to previous studies, the use of natural fibers has been increasing in recent years.[18-20] From the earliest construction based on clays, it has been known that natural fibers can be used to reinforce this type of structure. Over time, research has been conducted on the use of various fibers in the construction industry, including diss,[21] hemp,[22] banana fiber, kenaf, jute, barley, bagasse, totora, coconut, cotton, dates, durian, elephant grass, flax, palm, pineapple, cane, rice,

sansevieria, sisal, sunflower and bamboo,[23] among others.

Sugarcane bagasse fiber (CBF) is a solid lignocellulosic residue that remains after the extraction of juice from the stem of sugarcane, and is considered an agro-industrial waste. The production of between 101 and 340 million tons per year was estimated in 2012.[24] It has been reported that about 85% is used as fuel, although this practice results in severe environmental damage. There is therefore a strong need to find environmentally friendly alternatives for the exploitation of this type of waste, which would give it a greater economic value and make its use and application attractive.[25] It has been shown that when CBF is mixed with cement, the fiber delays the setting time and decreases the maximum temperature of hydration; this is due to its hygroscopic properties, defined as the ability to absorb and yield water through the mechanisms of absorption and capillarity.[26,27]

CBF waste is therefore an excellent candidate for use as reinforcement for concrete. Further advantages of using CBF include an increase in mechanical properties, with tensile strength values of between 170 and 290 MPa and an elasticity modulus between 15 and 25 GPa.[28,29]

In this study, we evaluated the integration, distribution and degradation of concrete specimens that had been modified by adding CBF to replace fine aggregate and exposed to aggressive media over a period of four years. The specimens were characterized structurally and morphologically to explore their possible application in hydraulic concrete-steel reinforcement systems. Chemical and structural assessments of the modified C-CBF samples (concrete with CBF) were evaluated by Fourier transform infrared spectroscopy (FT-IR), X-ray diffraction (XRD) and X-ray photoelectron spectroscopy (XPS), while the morphology, distribution and degradation of the samples were determined by scanning electron microscopy (SEM) and confocal laser scanning microscopy (CLSM).

EXPERIMENTAL

We evaluated modified specimens with and without the addition of 0.5 and 1 wt% of CBF, after exposing them to aggressive media for four years. These are referred to here as unmodified concrete (UC) and modified (C-CBF) samples, respectively. The aggressive conditions refer to immersion into seawater, sand saturated with seawater, and controlled atmosphere (85% relative humidity), which was achieved using a solution of H_2SO_4 at 5% v/v CBF with a particle size of 1.18 mm (#16).

Concrete specimens modified with 0.5 and 1 wt% CBF

The concrete specimens used in the experiments consisted of composite Portland cement (CPC), 30 RS (resistance class), the specifications of which are listed in Table 1, coarse aggregate, fine aggregate, and water (with a w/c ratio of 0.45).

To achieve good consistency and mixing of the material, the order of addition of these materials was as follows: 1) coarse aggregate, 2) fine aggregate, and 3) half of the water, in order to hydrate the aggregates. Cement was then added with one quarter of the water. When the mixture was homogenized, CBF was incorporated in the final mixing stage to prevent the remaining water from being absorbed, due to its hygroscopic property. CBF was added in proportions of 0.5 and 1 wt%, in relation to the fine aggregate (sand).

Table 1
Specifications of composite Portland cement (class 30 RS)[30]

Denotation	Components (% mass)					
	Portland clinker + plaster	Granulated blast furnace slag	Pozzolanic materials	Silica fume	Limestone	Minor components
Composite Portland cement (CPC)	50-94	6-35	6-35	1-10	6-35	0-5

Fourier transform infrared spectrometry

FT-IR measurements were performed in a Perkin Elmer Spectrum One instrument by direct transmittance using a KBr pellet, which is optically transparent and does not absorb energy in the IR, and CBF. To prepare the pellet, CBF (3%) was finely sprayed on an agate mortar until a homogeneous powder was obtained, and pulverized KBr (97%) was then added, mixed, and compressed at a pressure of 200 psi (lb/in^2). Each spectrum was recorded over 15 scans, in the range of 4000–650 cm^{-1}, with a resolution of 4 cm^{-1}. Background spectra were collected before

each sampling. The KBr was previously oven-dried to avoid interference due to the presence of water. The characteristic bands of cellulose and lignin were identified according to the literature.

X-ray photoelectron spectroscopy

Measurements were carried out under ultra-empty 10^{-10} Torr conditions in a modified Riber LDM-32 system with Auger (AES) and photoemission (XPS) electrons. The analysis chamber was equipped with a MAC-3 electron analyzer (CAMECA). XPS data were collected using the Kα Al line at a power of 1486.6 eV. The power scale was previously calibrated using the reference bond energies of Cu $2p_{3/2}$ at 932.67 eV and Ag $3d_{5/2}$ at 368.26 eV.

X-ray diffraction

X-ray diffractograms were recorded on a Bruker D8 Advance diffractometer using copper radiation (λ = 1.54 Å) generated at an applied voltage of 40 kV and a current of 40 mA. The samples were evaluated at intervals of 5° to 90° in 2θ, with a step size of 0.02°, over 60 min.

Confocal laser scanning microscopy (CLSM)

CLSM was used to analyze the cellulose and lignin autofluorescence of the modified (C-CBF) and reference (CBF) samples. 3D CLSM images were collected using a Zeiss LSM 710 (Carl Zeiss, Jena, Germany) confocal microscope, equipped with a Coherent Chameleon laser (Tisapphire). Measurements were made using transmitted light in the range of 400–700 nm, with four lasers (violet: 405 nm, blue: 488 nm, yellow: 561 nm, and red: 633 nm), and a working area of 5 mm^2. Chalcofluorine (1%) was used to dye the samples, which were left to rest for 5 min in the dark to determine whether cellulose was present.

Scanning electron microscopy

SEM was used to explore the morphology and distribution of the CBF in the concrete matrix. This was performed with a Hitachi S 4800 J instrument operating at 15 kV, using a backscattered electron detector. The samples were previously prepared by assembly with transparent resin (cold preparation). Subsequently, each sample was abraded with a silicon carbide denomination 600 sheet, and then polished with a 1 μm diamond paste. To perform X-ray microanalysis, the specimens were coated with graphite to make them conductive. A concrete fragment was metallized with gold to prevent electrical charging and allow better images to be obtained.

RESULTS AND DISCUSSION

Fourier transform infrared spectrometry

The IR spectrum obtained for the CBF is shown in Figure 1. A large number of bands can be observed, and the absorption bands for cellulose, hemicelluloses, and lignin overlap. It can be seen that CBF has wide absorption region bands at 3340 cm^{-1}, corresponding to the stretching of OH-alcohol groups of polysaccharides and OH-phenol in lignin. The band is centered at around 1723 cm^{-1}, corresponding to carbonyl bonds of the -C=O group present in aliphatic molecules, with weak but acute intensity. This is attributed to the stretching vibrations of the carboxylic acid of hemicelluloses. Likewise, in the fingerprint region, the presence of vibrations of glycosidic bonds in the range 1200–1037 cm^{-1} with medium and strong intensity is observed, indicating symmetrical and asymmetric stretching vibrations of the C-O and C-O-C groups that overlap with the vibrations of the -OH groups.

The absorption bands between 3000 and 2750 cm^{-1} are attributed to C-group stretching vibrations.[31] In the regions of 1400 and 1600 cm^{-1}, medium and weak intensity absorptions of the aromatic rings attributed to lignin were observed.[32]

According to the literature, the anomeric forms α and β of these polysaccharides absorb at approximately 1375 cm^{-1}. However, the most characteristic absorption band for the β configuration reported for cellulose is a weak band at approximately 894 cm^{-1}. Table 2 shows the main vibrational bands of CBF, CH_2, and CH_3, which are mainly present in the cellulose and hemicellulose structures.[32]

From contrast IR spectra (Fig. 2) for unmodified concrete (UC) and the modified specimen (C-CBF), it is observed that they have a similar structure. However, the UC sample has a higher transmittance compared to the modified specimen; that is, it absorbs more energy in the bands close to 3500 and 1000 cm^{-1}. Similarly, it can be observed that the C-CBF specimen shows a wider band in the region 3100–3600 cm^{-1} compared to concrete, which matches the OH^- vibration corresponding to portlandite ($Ca(OH)_2$). In addition, the shoulder and the bands located at 2969, 2874 and 2514 cm^{-1} correspond to the formation of calcium carbonate ($CaCO_3$). The shoulder masked at 1632 cm^{-1} of low intensity and present in the main band of strong intensity, centered around 1400–1600 cm^{-1}, corresponds to OH^- deformation of water. The band found at 1427 cm^{-1} corresponds to the C-O vibration of calcite. Finally, the band located between 890–1200 cm^{-1} corresponds to the overlap of silica vibrations (alita and gypsum).

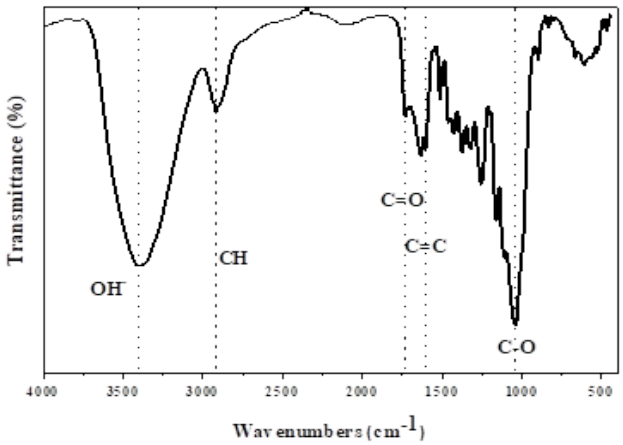

Figure 1: IR spectrum of CBF obtained by mechanical screening

Table 2
Main vibrational bands characteristic of CBF

Frequency (cm^{-1})	Intensity	Group	Assignment
894	Weak	C-H	Glycosidic β, stretching and deformation (cellulose)
1037	Strong	C-O	Symmetrical stretching
1161	Strong	C-O-C	Asymmetric stretching (cellulose, hemicelluloses)
1243	Strong	C=O	Stretching (lignin)
1317	Weak	CH_2	Oscillating vibration (cellulose)
1373	Weak	C-H	Deformation (cellulose, hemicelluloses)
1425	Weak	CH_2	Flexion (cellulose)
1520	Weak	C=C	Stretching aromatic ring (lignin)
1597	Stocking	C=C	Stretching aromatic ring (lignin)
1618	Stocking	O-H	Water absorption
1723	Weak	C=O	Stretching carboxylic acid and ketones (hemicelluloses)
2853	Weak	C-H	Symmetrical stretching (cellulose, hemicelluloses)
2937	Stocking	C-H	
3340	Strong	OH	Hydroxyl groups (cellulose, hemicelluloses)

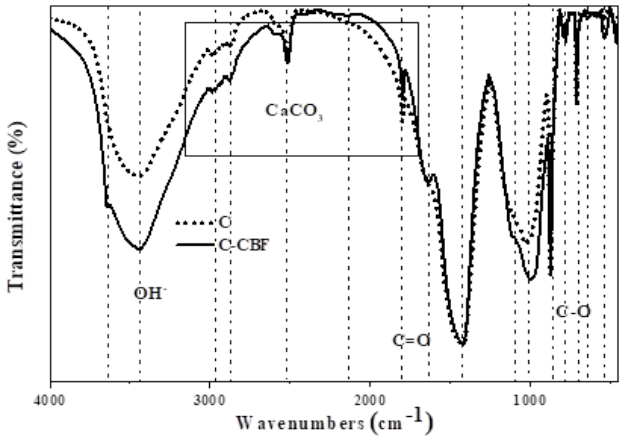

Figure 2: Comparison of IR spectra of UC and modified C-CBF

Similarly, the absorption bands around 710 cm^{-1} and 878 cm^{-1}, with medium and strong intensity, respectively, correspond to the vibrations of the C-O group. According to the literature, wavelengths of around 714 and 877–878 cm^{-1} belong to the vibrational modes ν_4 and ν_2 (flexion), which are attributed to the CO_3 groups present in the material. The low-intensity

bands centered around 400 and 800 cm^{-1} (fingerprint) are attributed to the presence of silicates, gypsum, and calcite, which are characteristic of cement.[33]

X-ray photoelectron spectroscopy

Figure 3 (a, b) presents the general XPS spectra for the analyzed samples (powders) of UC, C-CBF, and CBF, respectively. Peaks corresponding to oxygen (O1s), calcium (Ca2p), carbon (C1s), silicon (Si2p), and O KLL-1 Auger electrons are observed for the C-CBF and UC samples, which represent the energy of electrons ejected from atoms due to the filling of the O1s state in the K layer by an electron of the L layer together with the discharge of an electron from the L layer. In contrast, for the CBF, peaks corresponding to O, C, and Si elements are mainly observed, which are attributed to the composition of C and O base.

The significant presence of a shoulder at ligation energies of 290.0 eV in the XPS spectra for the UC and C-CBF samples (Fig. 3 a, b) was attributed to the presence of carbon in the form of carbonate (CO_3^{2-}). This shoulder is not shown in the XPS spectrum for CBF (Fig. 3 b). Table 3 displays the elemental compositions obtained using the XPS technique for CBF, UC, and C-CBF. The increases in the content of C, CO_3^{2-}, and Ca in the C-CBF specimen were attributed to the presence of carbonated material added to the concrete matrix. The C content of the CBF sample was approximately twice that of the UC and C-CBF specimens, and the oxygen content was significantly lower. We highlight the high CO_3^{2} content of the UC and the modified C-CBF samples.

The modified C-CBF showed a slight increase in the CO_3^{2-} group, which was an important result, as a high carbonate concentration is associated with a high compression resistance. Quantification was performed based on the peak intensity (or area) of the general spectrum, which is directly related to the atomic number generated in that peak.

$$N_A = I_A / S_A \quad (1)$$

where N_A is the atomic number, I_A is the peak area, and S_A is the sensitivity factor.

$$\%\,Atomic = \frac{N_A}{(N_A + N_B + N_C \ldots)} * 100 \quad (2)$$

The XPS high-resolution adjustment spectra for the C1s and O1s peaks observed at the outermost surface of the CBF (with a carbon offset of 284.5 eV) are shown in Figure 4a. The three components used in the C1s peak adjustment appear at bond energies close to 285, 286.5, and 288 eV, which are associated with carbon groups C-H /C-C, C-O, and C=O, respectively.[34,35]

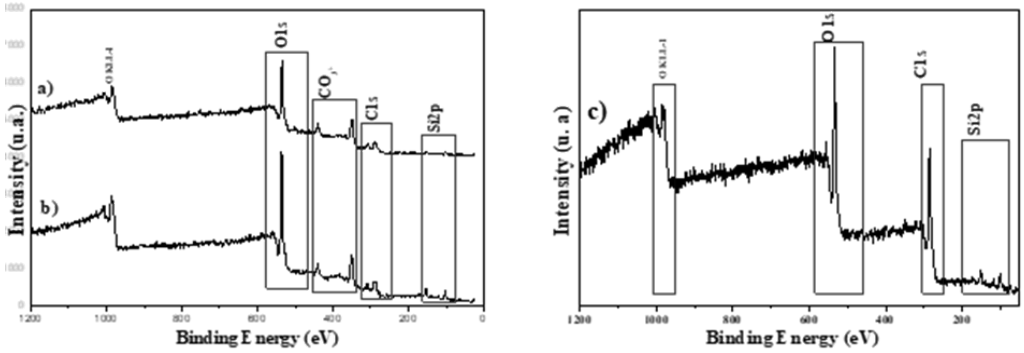

Figure 3: General XPS spectra a) C-CBF b) UC and c) CBF

Table 3
Atomic percentages observed by XPS for CBF, UC and C-CBF

Element	CBF	UC	C-CBF
O	33	54	49
Ca	0	9	12
Si	8	11	7
C	59	27	32
CO_3^{2-}	0	10	13

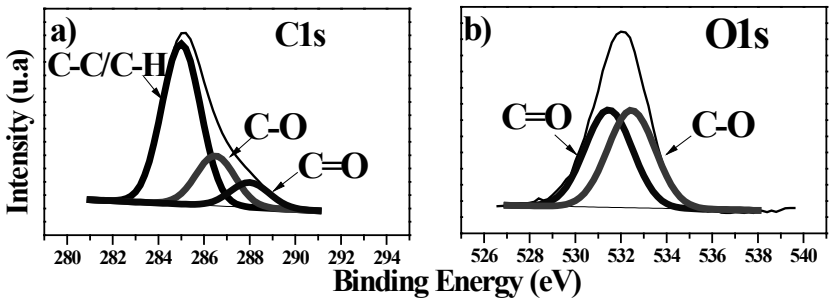

Figure 4: High-resolution XPS C1s and O1s spectra for the CBF

These correspond to the cellulose structures, hemicelluloses, and lignin present in the CBF, respectively, and validate the FT-IR results. Similarly, Figure 4b shows the two components used in the O1s peak adjustment that appear at bond energies near to 531.46 and 532.461 eV, corresponding to C=O and C-O groups, respectively, thus confirming the presence of carbon and oxygen base groups in the material.

X-ray diffraction

To investigate the changes in the crystallinity index and crystallite size, and to observe the behavior of CBF when in contact with concrete, XRD analysis of the modified C-CBF and UC specimens was performed. The CBF diffractogram is shown in Figure 5, and three reflections can be seen: a wide signal around 14.26°, and another around 22° in 2θ associated with an amorphous structure. This behavior arises because the cellulose contains a crystalline part, which is connected to disoriented amorphous regions,[36] as well as a reflection of very low intensity at 34.6°, which is characteristic of type α crystalline cellulose. According to the literature, cellulose has three characteristic signals at 16°, 22.5°, and 34.6° corresponding to the (110), (200), and (004) planes, respectively, whereas hemicelluloses have a reflection at 16°.[37] The crystallinity index and average crystallite sizes are frequently associated with modifications to the structure of lignocellulose after physicochemical pretreatments. It is therefore considered one of the most important factors determining the effect of the presence of fiber on the alkali hydrolysis reactions.

Figure 6 presents the diffractogram used for the analysis of the C-CBF and the UC samples. Indexing of the UC and the CBF samples was carried out separately to obtain the crystallographic charts corresponding to each material. It was possible to determine that there was no apparent chemical change or formation of a new species due to the addition of CBF.

However, spectral analysis of these materials revealed that the C-CBF showed an increase in intensity at the main peak, plane (104) corresponding to calcium carbonate. A slight displacement of the structure towards smaller angles in 2θ was also seen compared to UC, which was due to the changes in the position and interplanar distances from the addition of an organic material.

Table 4 shows the structural parameters calculated using the Scherrer equation,[38] which states that the grain size is inversely proportional to the average width of the maximum diffraction peak and the cosine of the angle of the maximum peak, and is given by:

$$D_p = \frac{K\lambda}{B\cos\theta} \quad (3)$$

where D_p is the crystal size, B is the average width of the peak considered for the calculation, θ is the angle corresponding to the peak maximum (2θ), λ is the X-ray wavelength (KαCu =1.5406 Å), and K is the form factor (0.94).

An analysis of the three-dimensional structures obtained for the CBF and C-CBF spectra showed a mutarotation of hydrogen in C-1, changing the structure of α CBF cellulose to *Iβ* cellulose, *i.e.*, from triclinic to monoclinic. The latter is the most stable structure and is commonly found in natural fibers (crystallographic chart: 00-056-1718), since the configuration *β*, together with all functional groups in equatorial positions, causes the cellulose molecular chain to extend in a more or less straight line, making it a good fiber-forming polymer.[39] This change is attributed to the hydrolysis reaction rate and the hydration temperature within the concrete matrix.

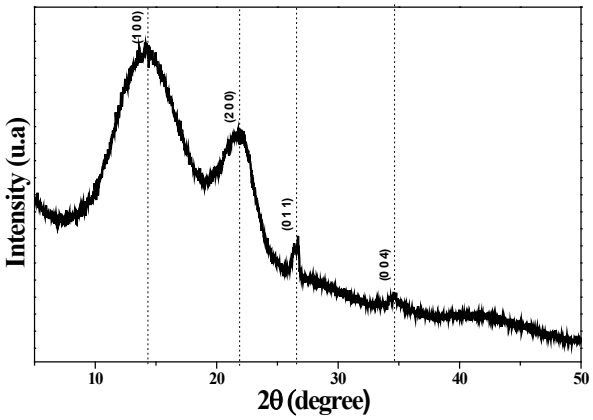

Figure 5: Diffractogram of CBF

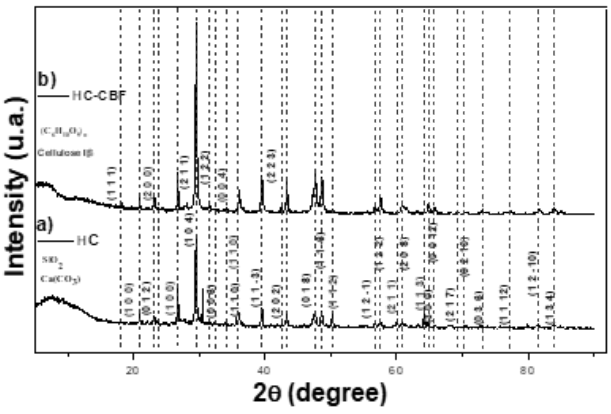

Figure 6: Diffractogram of UC (a) and C-CBF (b)

Table 4
Structural parameters obtained by XRD for UC and C-CBF

Sample	Xc (2Θ)	FWHM	Dp	Interplanar distance	Lattice parameter
UC	20.931	0.131	68.052	4.240	14.063
	23.127	0.383	23.499	3.842	12.744
	26.721	0.168	53.777	3.333	11.055
	29.489	0.211	43.175	3.026	10.037
	36.065	0.206	44.952	2.488	8.252
	39.513	0.240	39.062	2.278	7.557
	43.264	0.229	41.428	2.089	6.930
	47.528	0.488	19.759	1.911	6.339
	48.597	0.300	32.185	1.871	6.208
	57.503	0.285	35.301	1.601	5.311
C-CBF	20.919	0.122	73.470	4.242	14.072
	23.156	0.178	50.394	3.837	12.728
	26.717	0.144	62.931	3.333	11.057
	29.520	0.213	42.780	3.023	10.027
	36.087	0.185	49.950	2.486	8.247
	39.526	0.251	37.340	2.278	7.555
	42.484	0.075	125.682	2.126	7.051
	47.607	0.337	28.583	1.908	6.329
	48.623	0.313	30.854	1.871	6.205
	57.517	0.303	33.150	1.601	5.309

Confocal laser scanning microscopy

CLSM was used to characterize and identify the arrangements of cellulose and lignin in the sugarcane cell walls in the UC and C-CBF. Figure 7 (a-c) shows micrographs at 500 μm that were obtained via CLSM for the C-CBF samples exposed to different media over four years: through immersion into seawater, sand saturation with seawater, and a controlled atmosphere (85% HR).

The results obtained from fluorescent emission show that the C-CBF specimen exposed to the different media presented two different red and green signals in the spectral range 425–721 nm, where the color is attributed to the spectral region in which the sample is emitting. For the CBF, we observe two emission lines, green and red, which are attributed to the cellulose and regions rich in lignin, respectively.[40] Red and green emission lines were observed close to 597 nm and 520 nm, respectively, and were associated with the presence of Si II and Ca I, respectively, according to the literature.[41]

The micrography results (Fig. 8) showed a fluorescence emission signal at 463 nm, which was associated with the aromatic ring compound present in lignin, which forms part of the CBF. Absorption bands between 405 and 488 nm were associated with the presence of lignin in the material.[42]

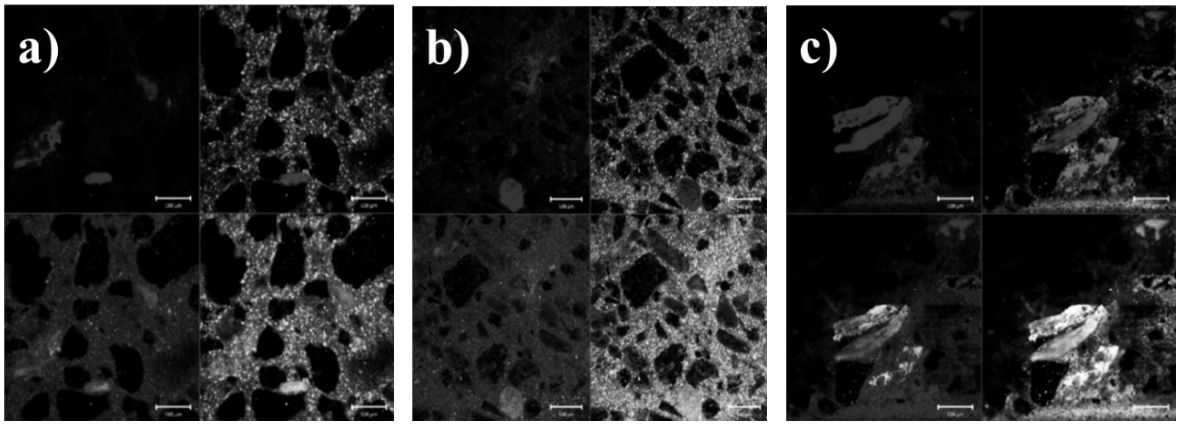

Figure 7: Micrographs of C-CBF specimens exposed in a) sediment, b) seawater and c) controlled atmosphere

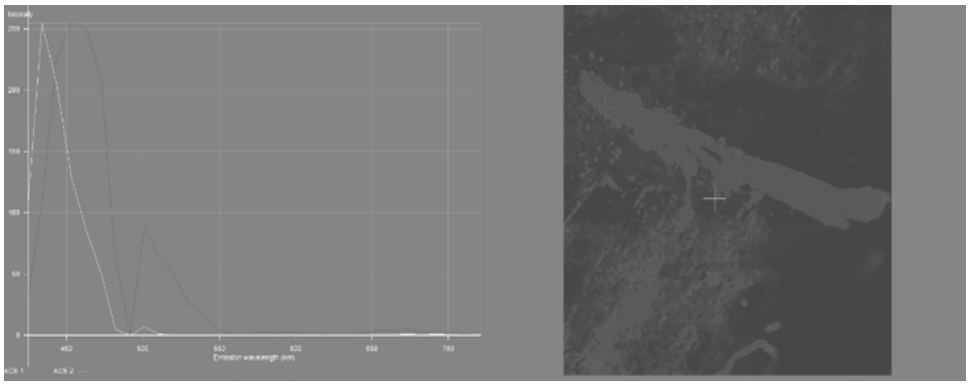

Figure 8: Emission lines observed for 0.5% CBF specimen exposed in controlled atmosphere

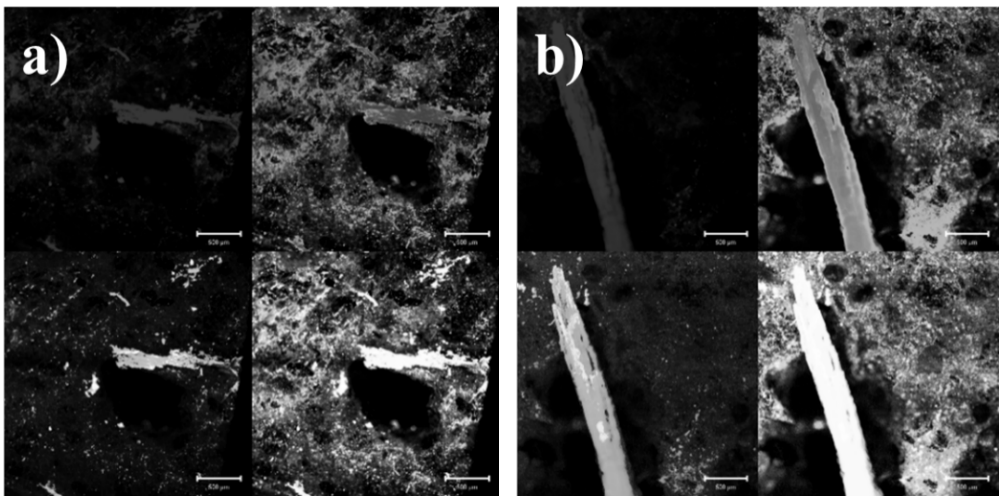

Figure 9: Chalcofluoride staining of C-CBF 0.5 and 1% of CBF exposed in a) controlled atmosphere and b) seawater

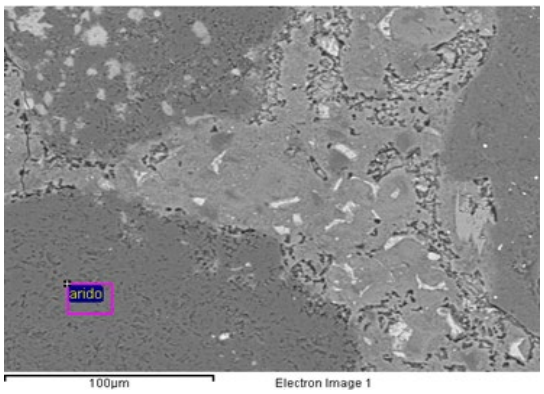

Figure 10: Micrograph of C-CBF with 1% CBF (100 µm)

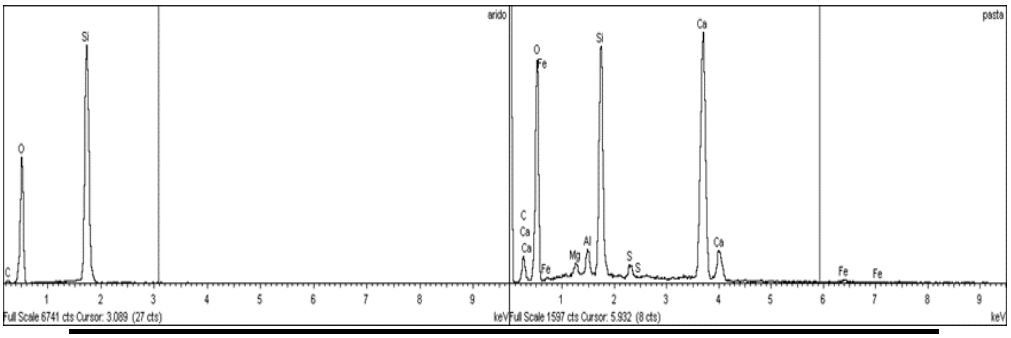

Spectrum	In stats	O	Mg	Al	Si	S	Ca	Fe	Total
Arid	Yes	56.96			43.04				100.00
Cement	Yes	54.89	0.64	1.31	12.71	0.99	28.51	0.95	100.00
Max.		56.96	0.64	1.31	43.04	0.99	28.51	0.95	
Min.		54.89	0.64	1.31	12.71	0.99	28.51	0.95	

Figure 11: Cementing matrix identification and chemical quantification by EDS microanalysis

We observed that the specimens with 1% CBF showed better CBF distribution within the UC. This was because there was a greater amount of material present, which caused stronger fluorescence signals in the system. We therefore ruled out the possibility that the CBF suffered degradation within the concrete matrix after four years of exposure. Figure 9 (a, b) shows micrographs of the specimens dyed with a white solution of chalcofluorine, which allows us to see the specific locations of the cellulose and lignin that make up the CBF. When the solution was added, the modified C-CBF specimen changed to a blue coloration, thereby confirming that the material contained cellulose and lignin, as the chalcofluoride is fixed to the cellulose cell walls, thus improving the image contrast under the microscope.

Scanning electron microscopy

The morphological distributions and changes in the C-CBF samples were examined by SEM and were compared to the UC samples. Figures 10-15 show scanning electron micrographs of a polished section of the modified concrete with 1% CBF, embedded in epoxy resin. All of the studied samples have a compact, rigid structure. Figure 10 presents an image obtained by backscattered electrons, where the cement grains are shown in different shades of gray, indicating areas of different compositions according to the average atomic number.

The darkest zone is related to arid or silica sand (dark gray), while the brightest zones represent the cement hydration products (light gray), and the brightest areas with the unhydrated cement grains when alkali hydrolysis reactions are carried out.[43,44] Chemical profiles were obtained through EDS analysis in order to observe the chemical composition and relative concentrations of the cementing matrix components,[45] which

resulted from the chemical reaction between the cement and the water through the hydration process (Fig. 11).

Figure 12 shows a micrograph obtained by secondary electrons (SE) of a sample of hardened (fractured) cemented paste, where the microstructure of the sine of the C-CBF can be seen in relation to w/c = 0.45. In general, the images of the CBF revealed that a dense layer of concrete paste covered the CBF, demonstrating excellent integration and good adherence between the CBF and the concrete. In this image, crystals of calcium hydroxide (CH) with hexagonal shapes, hydrated calcium silicate (CSH) along the basal plane, and ettringite (E), commonly represented in the form of needles, can be observed.[46]

The network of pores between the crystals was also visualized together with the distribution of the CBF on the cementing matrix. It was observed that the CBF was located in the concrete pores and was distributed evenly (Fig. 13).

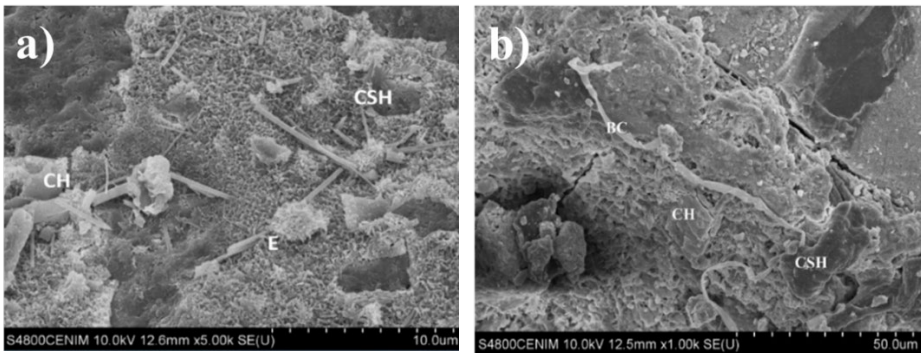

Figure 12: UC micrographs, ratio w/c = 0.45 C-CBF (1%), at a) 10 μm and b) 50 μm

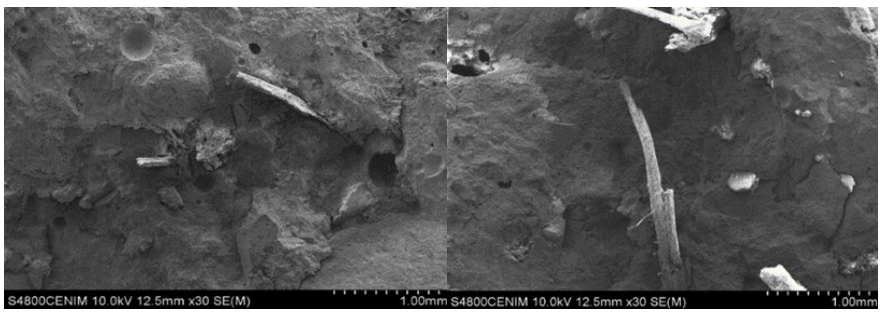

Figure 13: Fresh fracture micrograph corresponding to C-CBF (1%)

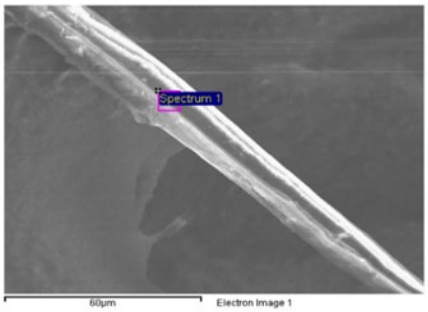

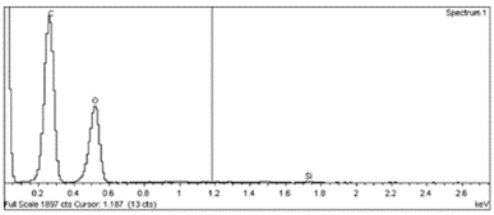

Spectrum	In stats.	C	O	Total
Spectrum 1	Yes	54.08	45.92	100.00
Mean		54.08	45.92	100.00
Std. deviation		0.00	0.00	
Max.		54.08	45.92	
Min.		54.08	45.92	

Figure 14: CBF micrograph (magnification: 60 μm) and its chemical profile performed by EDS analysis

A carbon fiber microanalysis at 60 μm was performed to confirm the presence of CBF within the concrete. Figure 14 shows an electronic image of the CBF obtained by backscattered electrons, and the results of the corresponding EDS analysis. The chemical composition of the fiber and the

component proportions can be observed, which mainly include carbon (C) and oxygen (O).

A freshly fractured C-CBF sample was metallized with gold in order to characterize the CBF distribution and morphology at a magnification of 1 μm. Figure 15a shows the modified paste with CBF,[17] where it can be seen that there is an interaction between the pore network and the cementation matrix with the CBF. An increase was made up to 1 μm (Fig. 15b) to observe the interface between the concrete and the CBF and to establish that there was no chemical interaction between them. This was because the carbon fiber was in a different region with respect to the cementitious paste. It can therefore be determined that the presence of organic material does not affect the alkali-hydrolysis reaction.

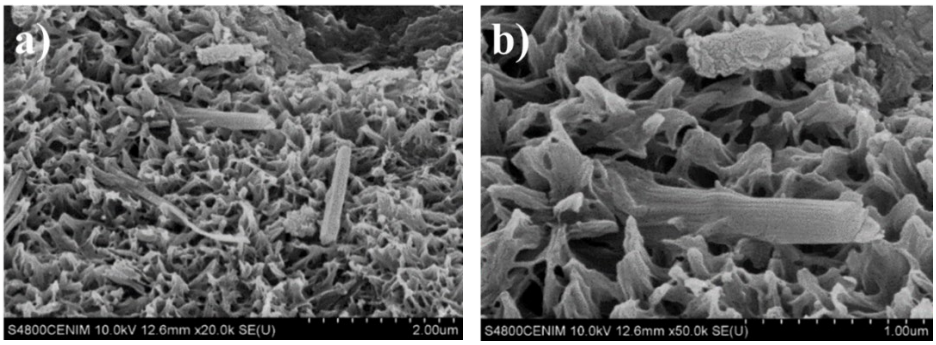

Figure 15: Micrographs of C-CBF (1%) exposed to controlled atmosphere a) magnification of 2 μm, b) magnification of 1 μm

CONCLUSION

In this study, structural and morphological characterization of CBF, UC and C-CBF samples was carried out. The aim was to determine the distribution, morphology and degradation of concrete samples previously modified with CBF as a partial replacement for fine aggregate, after exposure to aggressive media for four years. The following conclusions were drawn.

Based on the obtained SEM results, it was determined that the CBF was integrated into the concrete in a homogeneous way, without agglomeration of the CBF. Furthermore, the interaction that occurred during setting of the concrete was a physical one, and there was no evidence of any effect on the alkali-hydrolysis reactions of the concrete. However, using XRD, it was observed that the unmodified concrete showed a slight displacement of the characteristic signals compared to the specimen modified with CBF, toward smaller angles, which were associated with the heterogeneities of the CBF in the concrete paste.

The fluorescence observed from the CLSM results confirmed that the CBF distribution in the concrete was homogeneous, and that there was no physico-chemical degradation of the fiber after four years of exposure to three different types of aggressive media (controlled atmosphere, sediment, and seawater).

Finally, from a comparison of the high-resolution XPS spectra for the concrete in the presence and absence of CBF, it was observed that there were no significant differences in the analyzed surface, thus ruling out the formation of a new chemical species after the addition of CBF to the concrete. This finding supports both the SEM results and the XRD and FT-IR observations, since when each technique was used, the comparative spectra for the specimens with and without CBF had similar structures.

In summary, we found that CBF represents a viable alternative for incorporation as a substitute for fine aggregate in hydraulic concrete-steel reinforcement systems. The CBF distribution in the concrete was homogeneous, without agglomerations, and there was no physico-chemical degradation of the fiber after four years of exposure to aggressive media.

ACKNOWLEDGEMENTS: The present study was jointly supported by the Instituto Politécnico Nacional through projects SIP 20231307 and 20230611.

REFERENCES

[1] M. Henry and Y. Kato, *Resour. Conserv. Recycl.*, **82**, 86 (2014), https://doi.org/10.1016/j.resconrec.2013.10.012

[2] C. Meyer, *Cement Concr. Compos.*, **31**, 601 (2009), https://doi.org/10.1016/j.cemconcomp.2008.12.010

[3] J. Lehne and F. Preston, "Making Concrete Change Innovation in Low-Carbon Cement and Concrete", Chatham House Rep, 2018 pp. 1-122
[4] P. Van Den Heede and N. De Belie, *Cement Concr. Compos.*, **34**, 431 (2012), https://doi.org/10.1016/j.cemconcomp.2012.01.004
[5] B. Ambedkar, J. Alex and J. Dhanalakshmi, *Constr. Build. Mater.*, **148** 167 (2017), https://doi.org/10.5829/ije.2018.31.07a.02
[6] B. S. Thomas, S. Kumar and H. S. Arel, *Renew. Sustain. Energ. Rev.*, **80**, 550 (2017), https://doi.org/10.1016/j.rser.2017.05.128
[7] E. Y. Nakanishi, M. Frías and S. F. Santos, *J. Clean Prod.*, **116**, 236 (2016), https://doi.org/10.1016/j.jclepro.2015.12.113
[8] G. C. Cordeiro and K. E. Kurtis, *Cem. Concr. Res.*, **97**, 41 (2017), https://doi.org/10.1016/j.cemconres.2017.03.008
[9] S. Praveenkumar, G. Sankarasubramanian and S. Sindhu, *Build. Mater.*, **238**, 117 (2020), https://doi.org/10.1016/j.conbuildmat.2019.117691
[10] D. A. Adesanya and A. A. Raheem, *Constr. Build. Mater.*, **23**, 347 (2009), https://doi.org/10.1016/j.conbuildmat.2007.11.013
[11] C. C. Ban and M. Ramli, *Resour. Conserv. Recycl.*, **55**, 669 (2011), https://doi.org/10.1016/j.resconrec.2011.02.002
[12] L. Rodier, K. Bilba, C. Onesippe and M. A. Arsene, *Mater. Struct.*, **50**, 14 (2017), https://doi:10.1617/s11527-016-0958-6
[13] N. M. Al-Akhras and B. A. Abu-Alfoul, *Cem. Concr. Res.*, **32**, 859 (2002), https://doi.org/10.1016/S0008-8846(02)00716-0
[14] L. Rodier, E. Villar-Cociña and J. M. Ballesteros, *J. Clean Prod.*, **231**, 54 (2019), https://doi:10.1016/j.jclepro.2019.05.208
[15] J. M. L. Reis, *Constr. Build. Mater.*, **20**, 673 (2006), https://doi:10.1016/j.conbuildmat.2005.02.008
[16] M. Ardanuy, J. Claramunt and R. D. Toledo Filho, *Constr. Build. Mater.*, **79**, 115 (2015), https://doi:10.1016/j.conbuildmat.2015.01.035
[17] K. C. P. Faria, R. F. Gurgel and J. N. F. Holanda, *J. Environ. Manage.*, **101**, 7 (2012), https://doi:10.1016/j.jenvman.2012.01.032
[18] C. Asasutjarit, *Constr. Build. Mater.*, **21**, 277 (2007), https://doi:10.1016/j.conbuildmat.2005.08.028
[19] L. K. Aggarwal, *Cement Concr. Compos.*, **17**, 107 (1995), https://doi:10.1016/0958-9465(95)00008-Z
[20] A. Sellami, M. Merzoud and S. Amziane, *Constr. Build. Mater.*, **47**, 1117 (2013), https://doi.org/10.1016/j.conbuildmat.2013.05.073
[21] B. Çomak, A. Bideci and Ö. Salli Bideci, *Constr. Build. Mater.*, **169**, 794 (2018), https://doi.org/10.1016/j.conbuildmat.2018.03.029
[22] A. Sendra and J. Vercher, "Estudio comparativo de fibras naturales para reforzar hormigón", Universidad Politécnica de Valencia, 2020, pp. 1-80
[23] F. Luna Vera, H. A. Melo Cortes, C. V. Murcia and I. C. Galvis, *Informador Técnico*, **78**, 106 (2014), https://doi.org/10.23850/22565035.93
[24] N. El-Tayeb, *J. Mater. Process. Technol.*, **206**, 305 (2008), https://dx.doi.org/10.1016/j.matdes.2007.01.028
[25] K. G. Satyanarayana, J. L. Guimarães and F. Wypych, *Appl. Sci. Manuf.*, **38**, 1694 (2007), https://doi.org/10.1016/j.compositesa.2007.02.006
[26] S. R. Verma, *J. Mater. Environ. Sci.*, **3**, 1079 (2012)
[27] M. Mostafa and N. Uddin, *Build*, **5**, 282 (2015), https://doi.org/10.3390/buildings5010282
[28] Z. Li, X. Wang and L. Wang, *Appl. Sci. Manuf.*, **37**, 497 (2006), https://doi.org/10.1016/j.compositesa.2005.01.032
[29] Y. R. Loh, *Conserv. Recycl.*, **75**, 14 (2013), https://doi.org/10.1016/j.resconrec.2013.03.002
[30] ASTM C150/C150M-16, Standard Specification for Portland Cement, 2016, pp. 1-10
[31] P. Lu and Y.-L. Hsieh, *Carbohyd. Polym.*, **82**, 329 (2010), https://doi.org/10.1016/j.carbpol.2010.04.073
[32] D. Dai and M. Fan, *Mater. Sci. Appl.*, **1**, 336 (2010), https://doi.org/10.4236/msa.2010.16049
[33] M. Chollet and M. Horgnies, *Surf. Interface Anal.*, **43**, 714 (2011), https://doi.org/10.1002/sia.3548
[34] F. B. de Oliveira, *Ind. Crop. Prod.*, **93**, 48 (2016), https://doi.org/10.1016/j.indcrop.2016.04.064
[35] W. Cao, *Appl. Surface Sci.*, **389**, 404 (2016), https://doi.org/10.1016/j.apsusc.2016.07.095
[36] Y. Wang, *Biochim. Biophys. Acta*, **1773**, 863 (2007), https://doi.org/10.1016/j.bbamcr.2007.04.002
[37] P. M. Visakh and S. Thomas, *Waste Biomass Valoriz.*, **1**, 121 (2010), https://doi:10.1007/s12649-010-9009-7
[38] A. Monshi, M. R. Foroughi and M. R. Monshi, *World J. Nano Sci. Eng.*, **2**, 154 (2012), https://doi:10.4236/wjnse.2012.23020
[39] S. Kalia, *Int. J. Polym. Sci.*, **2011**, 1 (2011), https://doi.org/10.1155/2011/837875
[40] C. Sant'Anna, *Microsc. Res. Techn.*, **76**, 829 (2013), https://doi:10.1002/jemt.22235
[41] W. M. Haynes, "CRC Handbook of Chemistry and Physics", Taylor & Francis Group, 2014, pp 3-114
[42] C. Sant'Anna, *Microsc. Res. Techn.*, **76**, 829 (2013), https://doi:10.1002/jemt.22235
[43] P. Stutzman, *Cement Concr. Compos.*, **26**, 957 (2004), https://doi:10.1016/j.cemconcomp.2004.02.043
[44] S. Diamond, *Cement Concr. Res.*, **2**, 617 (1972), https://doi:10.1016/0008-8846(72)90115-9
[45] N. Thaulow, U. H. Jakobsen and B. Clark, *Cement Concr. Res.*, **26**, 309 (1996), https://doi:10.1016/0008-8846(95)00219-7
[46] K. L. Scrivener, *Cement Concr. Compos.*, **26**, 935 (2004), https://doi:10.1016/j.cemconcomp.2004.02.029